



HAL
open science

Design of Diamond Power Devices: Application to Schottky Barrier Diodes

Nicolas C. Rouger, Aurélien Maréchal

► **To cite this version:**

Nicolas C. Rouger, Aurélien Maréchal. Design of Diamond Power Devices: Application to Schottky Barrier Diodes. *Energies*, 2019, 12 (12), pp.2387. 10.3390/en12122387 . hal-02377365

HAL Id: hal-02377365

<https://hal.science/hal-02377365>

Submitted on 5 Nov 2020

HAL is a multi-disciplinary open access archive for the deposit and dissemination of scientific research documents, whether they are published or not. The documents may come from teaching and research institutions in France or abroad, or from public or private research centers.

L'archive ouverte pluridisciplinaire **HAL**, est destinée au dépôt et à la diffusion de documents scientifiques de niveau recherche, publiés ou non, émanant des établissements d'enseignement et de recherche français ou étrangers, des laboratoires publics ou privés.

Article

Design of Diamond Power Devices: Application to Schottky Barrier Diodes

Nicolas Rouger ^{1,*}  and Aurélien Maréchal ²

¹ LAPLACE, Université de Toulouse, CNRS, 31000 Toulouse, France

² University Grenoble Alpes, CNRS, Grenoble INP, G2Elab, 38000 Grenoble, France; aurelien.marechal@g2elab.grenoble-inp.fr

* Correspondence: nicolas.rouger@laplace.univ-tlse.fr

Received: 17 May 2019; Accepted: 18 June 2019; Published: 21 June 2019



Abstract: Owing to its outstanding electro-thermal properties, such as the highest thermal conductivity (22 W/(cm·K) at room temperature), high hole mobility (2000 cm²/(V·s)), high critical electric field (10 MV/cm) and large band gap (5.5 eV), diamond represents the ultimate semiconductor for high power and high temperature power applications. Diamond Schottky barrier diodes are good candidates for short-term implementation in power converters due to their relative maturity. Nonetheless, diamond as a semiconductor for power devices leads to specificities such as incomplete dopant ionization at room temperature and above, and the limited availability of implantation techniques. This article presents such specificities and their impacts on the optimal design of diamond Schottky barrier diodes. First, the tradeoff between ON-state and OFF-state is discussed based on 1D analytical models. Then, 2D numerical studies show the optimal design of floating metal rings to improve the effective breakdown voltage. Both analyses show that the doping of the drift region must be reduced to reduce leakage currents and to increase edge termination efficiency, leading to better figures of merit. The obtained improvements in breakdown voltage are compared with fabrication challenges and the impacts on forward voltage drop.

Keywords: diamond; power devices; Schottky barrier diodes; wide bandgap semiconductors; modelling

1. Introduction

During the last decade, wide bandgap power devices have been successfully developed. One of the key benefits of wide bandgap power devices is to reach the same conduction losses with unipolar devices as those of legacy bipolar Silicon power devices. Due to the unipolar conduction of wide bandgap power devices, switching losses are much lower than those of Silicon bipolar devices (e.g., “zero” recovery current, no tail current). Among the multiple developed device architectures, SiC MOSFETs, diodes and GaN HEMTs are commercially available, offering significant improvements in the efficiency vs. power density tradeoff. In this context, diamond is expected to improve the system-level benefits of wide bandgap power devices in power converters. Indeed, diamond has a critical electric field as high as 10 MV/cm, high hole mobility (2000 cm²/(V·s)) and the highest thermal conductivity (22 W/(cm·K) at room temperature), offering (theoretically) the best performance. Nonetheless, diamond still faces a number of challenges which currently limit the experimental figures of merit of diamond power devices. Such challenges are typically the incomplete dopant ionization due to deep donor and acceptor levels, management of high electric fields and voltage breakdown mechanisms, growth of high quality and low defects monocrystalline diamond, the lack of material maturity, and the understanding and improvements on the oxide-diamond interface. So far, the most mature diamond devices are Schottky diodes. In this context, this article highlights the design trade off applied to diamond and diamond Schottky diodes in particular. The design of the diamond drift

region and its combination with the Schottky barrier behavior is detailed. In order to reach better figure of merits with diamond power devices, it is of the highest importance to reach an experimental breakdown voltage which is as close as possible to the theoretical 1D breakdown voltage. Hence, dedicated junction terminations are required, related with the specificities of diamond (e.g., large electric field values and gradients). This article is organized as follows. Section 2 presents a brief review of diamond diodes where the architectures and the performances are shown. Section 3 discusses the ON-state versus OFF-state trade off of diamond Schottky barrier diodes. Section 4 presents numerical simulations to improve the 2D breakdown voltage. The design trade-offs are discussed, based on a case study at 1 kV. Finally, key results are summarized and future studies are introduced.

2. Brief Review of Diamond Diodes

Tremendous achievements have been made in substrate crystalline quality, and devices have been fabricated demonstrating the high potential of diamond for power electronics applications. However, in order to meet the power systems requirements, efforts are required to improve the voltage and current ratings of the devices. Nowadays, diamond diodes are the most mature/advanced power switches for integration into power systems.

Since the first development of diamond Schottky barrier diodes (SBDs) in the early 1990s [1–3], high breakdown voltages of 10 kV [4], high electric field of $7.7 \text{ MV}\cdot\text{cm}^{-1}$ [5], good switching properties [6–8] and elevated operating temperatures ($>250 \text{ }^\circ\text{C}$) have been reported. However, non-uniformities in the material quality (substrate and homoepitaxial diamond layers) have resulted in discrepancies between the reported results. Moreover, the breakdown of such devices is mainly due to the increase of leakage currents rather than by a 1D-avalanche breakdown. In fact, there is a clear lack of efficient edge termination structures to avoid the premature breakdown of the devices. Cross-sectional views of several diamond diode architectures which have been reported in the literature are summarized in Figure 1, and their properties are listed in Table 1. Vertical structures are the most convenient for power electronics applications in terms of scalability, larger area and better electric field management. Currents as high as 20 A and operating temperature of $200 \text{ }^\circ\text{C}$ are reported on such packaged vertical diamond SBDs [9]. However, a complex thinning process of the conductive HPHT substrate is required to obtain such high currents, which is detrimental for large-scale applications. The lack of highly-conductive, large area freestanding diamond substrates motivated the development of pseudo-vertical diamond SBD.

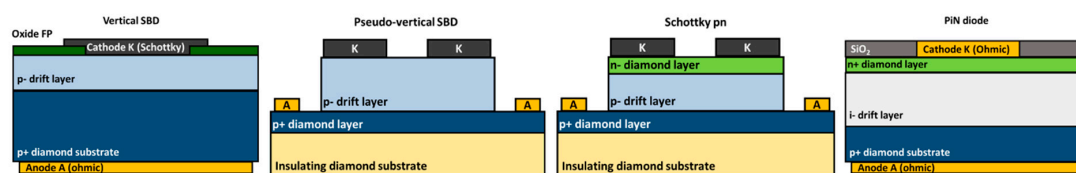


Figure 1. Cross sectional views of various unipolar and bipolar diamond diode architectures for power electronic applications. Vertical Schottky barrier diode with oxide field plate [10], pseudo-vertical SBD [5], Schottky pn diode [11] and PiN diode [12].

Table 1. State of the art properties of various diamond diodes (at 300K). Bold values represent better performance.

Device	Vertical SBD	Pseudo-Vertical SBD	Schottky pn Diode	PiN Diode
Conduction type	Unipolar	Unipolar	Unipolar	Bipolar
$BV^2/R_{on}S$ (MW·cm ⁻²)	25 [13]	166.7 [5]	30.25 [11]	2.9 [12]
BV (V)	1.8 kV [10]	1.6 kV [14]	55 V [11]	920 V [12]
On state current density (A·cm ⁻²)	3 kA·cm ⁻² at V = 8 V [10]	1 kA·cm ⁻² at V = 6 V [5]	60 kA·cm⁻² at V = 6 V [11]	15 kA·cm ⁻² at 35 V [15]
Switching speed	1.5 V·ns ⁻¹ at 20 A·μs ⁻¹ [8]	16 V·ns⁻¹ 100 V and 200 mA [16]	Turn off speed ≈ 10 ns [6], lack of information	6 V·ns ⁻¹ at 4 A·μs ⁻¹ [7]

The pseudo-vertical SBD consisting of a heavily boron-doped layer first grown on a high crystalline quality electrically insulating monocrystalline diamond substrate on top of which a low boron-doped layer is deposited makes it possible to increase the trade-off between the ON- and the OFF-state operation. The drift layer is etched down to the p+ layer in order to deposit the ohmic contact directly on top of the low resistivity layer. In this structure, the electrical current flows vertically in the drift layer and laterally in the p+ layer. However, the total current is limited with this design due to the lateral current flow in the p+ layer. Interactions between diodes are also observed using this design [17]. Nevertheless, good properties are obtained such as high current density and high breakdown voltage [5]. Moreover, good switching properties on such diodes are reported with dV/dt in the order of 10 V/ns [16]. On the other hand, the pseudo-vertical structure is limited to BV in the order of 3 kV due to the limitation of the etching process.

The highest current density (10^4 A·cm⁻² at 6 V) reported for a diamond diode was achieved using the Schottky pn diode structure [11,18]. It consists of a Schottky metal deposited on top of a thin n-type diamond layer which is fully depleted in both ON- and OFF-state operation. The advantage of this structure is the absence of trade-off between $R_{on}S$ and BV [11,19]. However, the n-type layer thickness is also the limiting factor for reaching high BV.

PiN diodes are composed of a low boron-doped diamond drift layer sandwiched between an n+ type layer and a p+ type layer. The use of heavily doped n+ and p+ type layers reduces the resistivity thanks to the hopping conduction mechanism. The ON-state operation is based on the conductivity modulation in the base region, i.e., the injection of minority carriers into the drift layer. Even though the electrical transport in the drift layer is unknown, high current density, high BV with positive temperature coefficient, high temperature operation and fast switching operation are reported [7,12,15,20]. Nonetheless, bipolar diamond diodes will be competitive only at high breakdown voltages (>10 kV), associated to longer carrier lifetimes (>10 ns), to compensate the high built-in potential (around 4.7 V) due to the wide bandgap of diamond. Hence, a focus is done here on unipolar diamond diodes, which are good candidates for short-term system-level implementation.

The performances in the ON- and OFF-states of the aforementioned devices are strongly dependent on the drift region design. There is a trade-off between the ON-state losses represented by the specific ON-state resistance $R_{on}S$ and the BV, i.e., there is only one drift region design (doping and thickness) which minimizes the ON-state losses for a given BV and operating temperature [21] as discussed in the next section. The effect of the Schottky barrier in this trade-off will be also further discussed.

3. ON-State Versus OFF-State Trade-Off

In high voltage power devices, the drift region is responsible for most of the ON-state conduction losses. Indeed, the drift region is lightly doped and thick enough to offer a high blocking voltage. Hence, its resistance is typically higher than other sources of total series resistance (e.g., due to the contacts, channel region or substrate). In Silicon, 95% of the ON-state voltage drop in vertical

600V MOSFETs is due to the sole drift region [22]. In bulk diamond, Figure 2 shows the specific ON-state resistance $R_{on,S}$ of a vertical drift region as a function of breakdown voltage predicted by 1D avalanche model [21,23] and for a Non Punch Through condition (NPT). This specific ON-state resistance is the lowest possible with unipolar vertical diamond power devices having a breakdown voltage between 1kV and 10kV. For a 10kV breakdown voltage and at 500 K, the specific on state resistance is reduced to $60\text{m}\Omega\cdot\text{cm}^2$ with diamond at 500 K, whereas it is $210\text{m}\Omega\cdot\text{cm}^2$ and $170\text{m}\Omega\cdot\text{cm}^2$ respectively for vertical n-type GaN and 4H-SiC. This comparison currently underestimates the benefits of diamond, since the peak electric field for thick and lightly doped drift regions can be further improved. In this plot, a p-type diamond drift region is considered as presented in Figure 1, since Boron doping and holes as majority carriers have proven to maximize the diamond conductivity [24,25]. In the case of n-type diamond drift regions, the typical dopants would be Phosphorus or Nitrogen, but both the extremely deep donor levels (0.57 eV and 1.7 eV, respectively) make such options almost unsuitable for power electronics applications. For the prediction of the specific ON-state resistance, up to date models have been used [25]: incomplete Boron ionization (with doping and temperature dependence: Equations (1)–(3) with p the hole concentration), hole mobility in CVD diamond (with doping and temperature dependence: Equations (4)–(6)) and the drift region thickness set as the thinnest possible after reaching NPT condition in OFF-state as predicted by 1D impact ionization integral [21]. As in [25], the physical parameters were set to $g_h = 0.25$, $N_v = 2.17 \times 10^{19}\text{ cm}^{-3}$, $\beta_{min} = 0$, $\beta_{max} = 3.11$, $N\beta = 4.1 \times 10^{18}\text{ cm}^{-3}$, $\gamma\beta = 0.617$, $\mu_{min} = 0$, $\mu_{max} = 2016\text{ cm}^2/(\text{V}\cdot\text{s})$, $N\mu = 3.25 \times 10^{17}\text{ cm}^{-3}$, $\gamma\mu = 0.73$. In Equation (1), N_A is the Boron doping concentration and N_D the compensation (assumed to be negligible). The doping of the drift region is calculated by the 1D ionization integral in NPT condition, where one breakdown voltage leads to a unique drift region doping. The doping compensation is neither taken into account nor its effect on the mobility of free holes [26]. Due to the incomplete ionization of Boron in diamond, the number of free holes is dramatically increased at temperatures above room temperature, while their mobility is reduced at higher temperatures [27]. Consequently, the specific ON-state resistance of p-type Boron-doped diamond drift regions exhibits a Negative (NTC) then Positive (PTC) Temperature Coefficient [28], above room temperature. Therefore, there is an “optimal” temperature at which the increased number of holes is compensated by their lower mobility. Consequently, the specific ON-state resistance exhibits a global minimum at such “optimal” temperatures, as a function of the doping level and consequent breakdown voltage in NPT condition. Table 2 summarizes the design and key parameters of the diamond drift region according to the previous assumptions.

$$p = \frac{1}{2}(\Phi_a + N_D) \left(\sqrt{1 + \frac{4\Phi_a(N_A - N_D)}{(\Phi_a + N_D)^2}} - 1 \right) \quad (1)$$

$$\Phi_a = g_h \cdot N_v \exp\left(-\frac{E_a}{k_B T}\right) \quad (2)$$

$$E_a(\text{eV}) = 0.38 - 4.7877 \times 10^{-8} \times N_A^{1/3} \quad (3)$$

$$\mu(T, N_A) = \mu(300, N_A) \times \left(\frac{T}{300}\right)^{-\beta(N_A)} \quad (4)$$

$$\beta(N_A) = \beta_{min} + \frac{\beta_{max} - \beta_{min}}{1 + \left(\frac{N_A}{N_\beta}\right)^{\gamma_\beta}} \quad (5)$$

$$\mu(300, N_A) = \mu_{min} + \frac{\mu_{max} - \mu_{min}}{1 + \left(\frac{N_A}{N_\mu}\right)^{\gamma_\mu}} \quad (6)$$

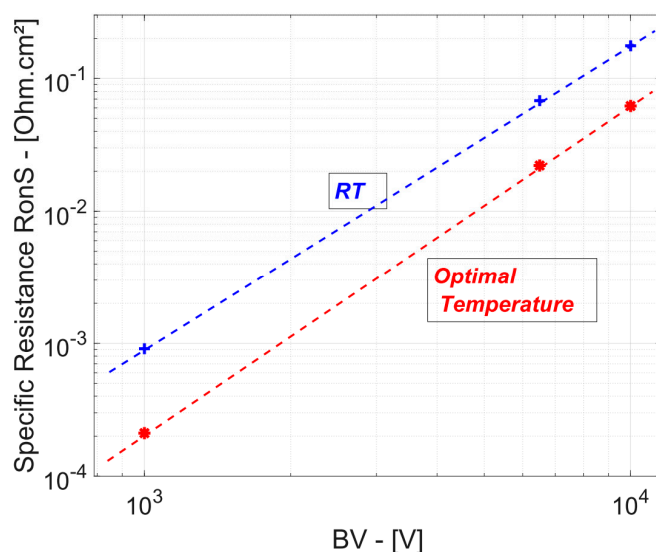


Figure 2. Specific ON-state resistance in bulk Diamond as a function of breakdown voltage and temperature (NPT condition).

Table 2. Key parameters of the diamond P-type Boron-doped drift region as a function of breakdown voltage in NPT condition.

	1 kV	6.5 kV	10 kV
Drift region Boron doping	$1.8 \times 10^{17} \text{ cm}^{-3}$	$5.5 \times 10^{15} \text{ cm}^{-3}$	$2.7 \times 10^{15} \text{ cm}^{-3}$
Drift region thickness in NPT condition	1.75 μm	27 μm	48 μm
RonS at Room Temperature	0.85 $\text{m}\Omega\cdot\text{cm}^2$	70 $\text{m}\Omega\cdot\text{cm}^2$	180 $\text{m}\Omega\cdot\text{cm}^2$
“Optimal” Temperature minimizing RonS	660 K	540 K	500 K

The previous introduction considered a NPT condition and a breakdown voltage predicted by 1D impact ionization integral. As it will be described hereinafter, the breakdown voltage in diamond devices and in diamond SBDs in particular is currently mostly governed by excessive leakage currents and premature breakdown due to poor electric field management. Moreover, the NPT condition does not lead to the minimum specific ON state resistance for each breakdown, since there is an optimal punch through coefficient under PT condition [21]. For all these reasons, four different designs of the drift region will be considered—see Figure 3a,b and Table 3—for a 1D breakdown voltage of 1 kV (as predicted by impact ionization integral based on temperature independent impact ionization coefficients in CVD diamond from [23]). The NPT design has the highest 1D peak electric field (10 MV/cm at breakdown) and the highest “optimal” temperature (660 K) which minimizes the specific ON-state resistance. The lowest specific ON-state resistance is obtained at 650 K for the optimal PT design, whereas lower doping leads to increased specific ON-state resistances and lower “optimal” temperature. The “optimal” temperature can also be seen as the temperature threshold between NTC and PTC, which is an important parameter for the system-level design.

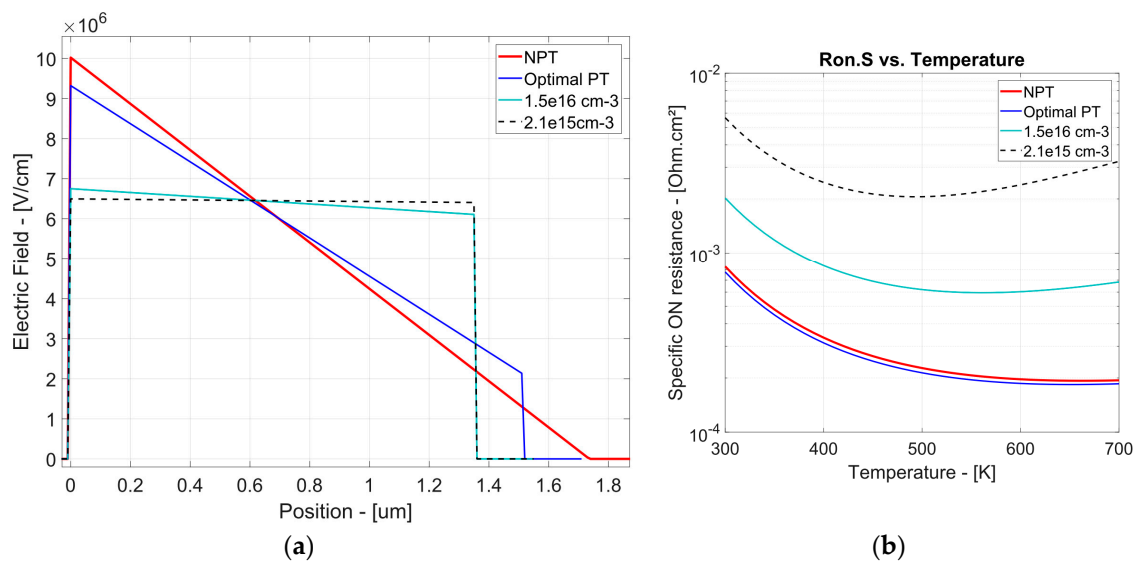


Figure 3. (a) 1D Electric field distribution at the avalanche breakdown, for four drift region designs. (b) Specific ON-state resistance as the function of the temperature, for four different designs of a 1 kV diamond drift region.

Table 3. Key parameters of the diamond p-type Boron-doped drift region for a designed breakdown voltage of 1 kV.

	Design Drift #a	Design Drift #b	Design Drift #c	Design Drift #d
	1 kV NPT	1 kV Optimal PT	1 kV lower doping	1 kV lightly doped
Drift region Boron doping	$1.8 \times 10^{17} \text{ cm}^{-3}$	$1.5 \times 10^{17} \text{ cm}^{-3}$	$1.5 \times 10^{16} \text{ cm}^{-3}$	$2.1 \times 10^{15} \text{ cm}^{-3}$
Drift region thickness in NPT condition	1.75 μm	1.51 μm	1.35 μm	1.35 μm
Peak electric Field	10 MV/cm	9.3 MV/cm	6.75 MV/cm	6.5 MV/cm
R_{onS} at Room Temperature	0.85 $\text{m}\Omega\cdot\text{cm}^2$	0.77 $\text{m}\Omega\cdot\text{cm}^2$	2 $\text{m}\Omega\cdot\text{cm}^2$	5.5 $\text{m}\Omega\cdot\text{cm}^2$
R_{onS} at optimal temperature	0.195 $\text{m}\Omega\cdot\text{cm}^2$	0.183 $\text{m}\Omega\cdot\text{cm}^2$	0.6 $\text{m}\Omega\cdot\text{cm}^2$	2 $\text{m}\Omega\cdot\text{cm}^2$
“Optimal” Temperature minimizing R_{onS}	660 K	650 K	560 K	490 K

In the case of diamond SBDs, the effect of the Schottky barrier height (Φ_b) must be considered on the compromise between ON-state losses and OFF-state capability (leakage current, OFF-state power loss and 3D electric field distribution at breakdown). Coupled with the design of the drift region, the effective Schottky barrier height must be carefully designed, while taking into account the leakage current in OFF-state, the forward voltage drop and their dependence on bias and temperature [5,29]. For the OFF-state analysis, the thermionic field emission (TFE) leakage current is considered, with the Schottky barrier lowering effect, as already presented in [29–31]. The multiplication of the TFE leakage current due to avalanche is not taken into account. Figure 4 presents the reverse characteristics of 1 kV diamond SBDs at 500 K junction temperature, using the boron doping levels of Table 3. The initial Schottky Barrier height has been set to 1.7 eV, as previously obtained using Mo/Pt/Au metal stack on Oxygen terminated CVD diamond in [32]. The effective barrier height is a function of the metal work function, the diamond surface and the Schottky contact annealing. In the case of Zr/Oxygen terminated CVD diamond, the initial Schottky Barrier height is comprised between 0.88 eV (high temperature annealing) and 1.84 eV (as deposited) [31]. The effective Schottky barrier height is highly dependent on the fabrication process. The Richardson constant has been set at $A^* = 90 \text{ A}\cdot\text{cm}^{-2}\cdot\text{K}^{-2}$ as in [29–31]. The purpose of this analytic model is to highlight the design trade-off and the specificities of diamond SBDs. Although higher doping levels lead to lower specific ON-state resistances (see Table 3),

the leakage currents for Design Drift #a and #b are too high: for a drift region doping of $1.5 \times 10^{17} \text{ cm}^{-3}$ (design drift #b), the leakage current density is higher than $1 \text{ A}\cdot\text{cm}^{-2}$ at 200 V, leading to $200 \text{ W}\cdot\text{cm}^{-2}$ OFF-state loss density. The predicted avalanche breakdown of 1 kV cannot be obtained, and a premature breakdown would occur between 100 V and 200 V due to thermal runaway in OFF-state. On the other hand, the leakage current density and power loss density of lower doped drift regions (Drift design #c and #d) lead to leakage currents lower than $1 \text{ mA}\cdot\text{cm}^{-2}$ at 1 kV. Figure 5 shows the forward characteristics of such diamond diodes, for the different drift region doping levels. A doping of $1.5 \times 10^{16} \text{ cm}^{-3}$ (Drift design #c) is clearly the best compromise between OFF-state and ON-state, even at a high temperature of 500 K. Decreasing the Schottky barrier height to 1.55 eV will further improve the compromise between the forward voltage drop and the OFF-state leakage level (blue curves in Figure 5a,b). Improvements on the metal/diamond interface leading to a lower ideality factor of 1.2 is also plotted in Figure 5, highlighting the possible short-term performances of 1 kV class diamond SBDs. An active area of $1.18 \times 1.18 \text{ mm}^2$ has been set in Figure 5b, similar to a commercially available 1200 V 2 A SiC “Schottky” diode (i.e., Wolfspeed CPW4-1200-S002B 1200V [33]). At 500 K and $500 \text{ W}\cdot\text{cm}^{-2}$ power loss density in ON-state, the current density (total current) of three different Schottky barriers on $1.5 \times 10^{16} \text{ cm}^{-3}$ Boron-doped diamond (design drift #c) are $335 \text{ A}\cdot\text{cm}^{-2}$ (4.7 A) at 1.49 V, $283 \text{ A}\cdot\text{cm}^{-2}$ (3.96 A) at 1.77 V, and $254 \text{ A}\cdot\text{cm}^{-2}$ (3.6 A) at 1.97 V, respectively for ($n = 1.2$, $\Phi_b = 1.55 \text{ eV}$), ($n = 1.5$, $\Phi_b = 1.55 \text{ eV}$) and ($n = 1.5$, $\Phi_b = 1.7 \text{ eV}$). These biasing conditions are highlighted by the filled circles in Figure 5a,b. The dependence of the forward characteristics with temperature is presented in Figure 6a,b for the design drift #c and the ($n = 1.2$, $\Phi_b = 1.55 \text{ eV}$) Schottky barrier. The high current densities and low forward voltage drop presented in Figure 6b can be obtained in applications with small or medium duty cycle values (<0.5), to comply with a thermal power loss density in the order of 100 to $500 \text{ W}\cdot\text{cm}^{-2}$. Although the performance of such a diode is clearly attractive at high temperatures ($>400 \text{ K}$), the forward voltage drop has a NTC, even at high current densities ($<1800 \text{ A}\cdot\text{cm}^{-2}$ or $4 \text{ kW}\cdot\text{cm}^{-2}$) and high temperatures ($<640 \text{ K}$). This NTC behaviour will affect the ability to increase the current capability by paralleling diamond devices in power converters. However, one should note that diamond has the highest thermal conductivity among typical power semiconductors, and paralleling at the sample level should not be an issue, albeit additional specific electro-thermal-mechanical studies must be done. For a diamond Schottky SBD, its thermal stability and surge capability with this NTC behaviour must also be further assessed, with possible benefits on these aspects.

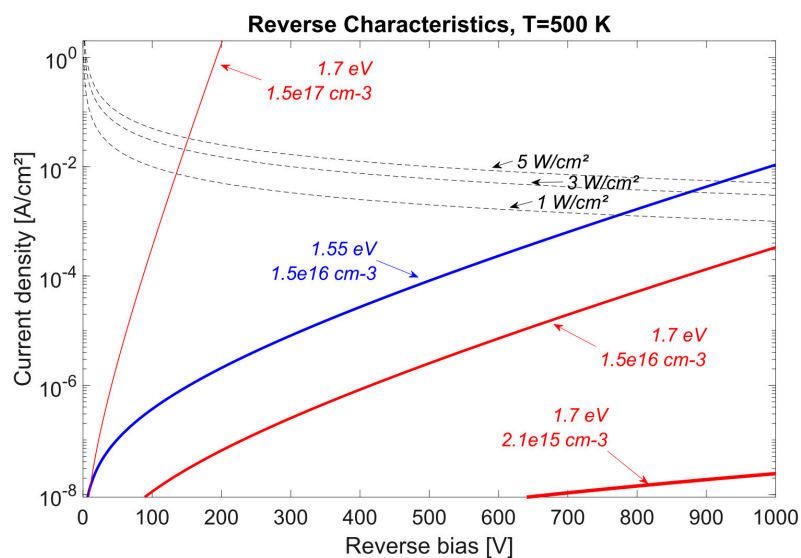


Figure 4. Reverse characteristics at 500 K of Boron-doped diamond SBDs, for different drift region designs (1 kV predicted avalanche breakdown). The dotted plots indicate a thermal power loss density of 1% the ON-state power loss density.

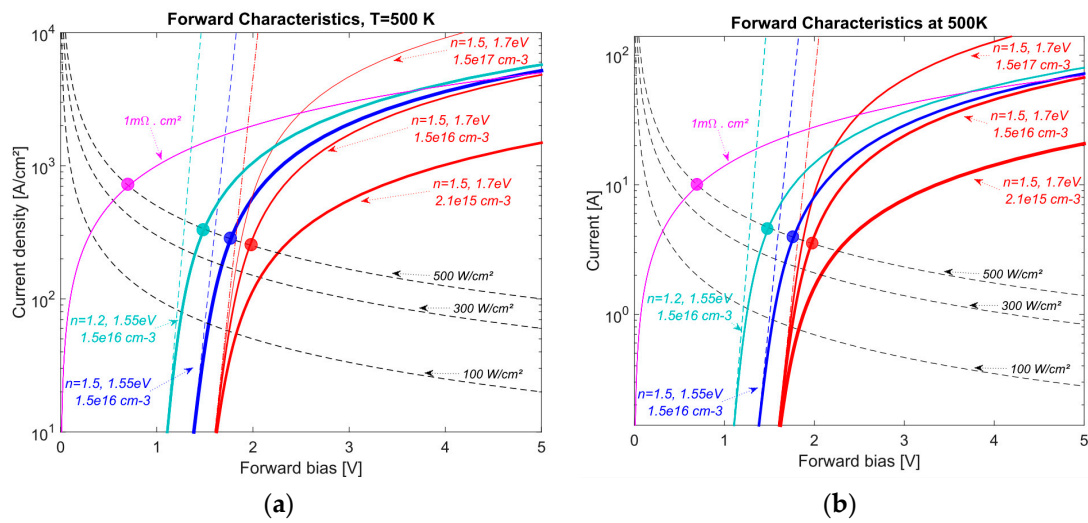


Figure 5. Forward characteristics at 500 K for different diamond SBDs. (a) Current density. (b) Forward current for an active area of 1.18 mm × 1.18 mm.

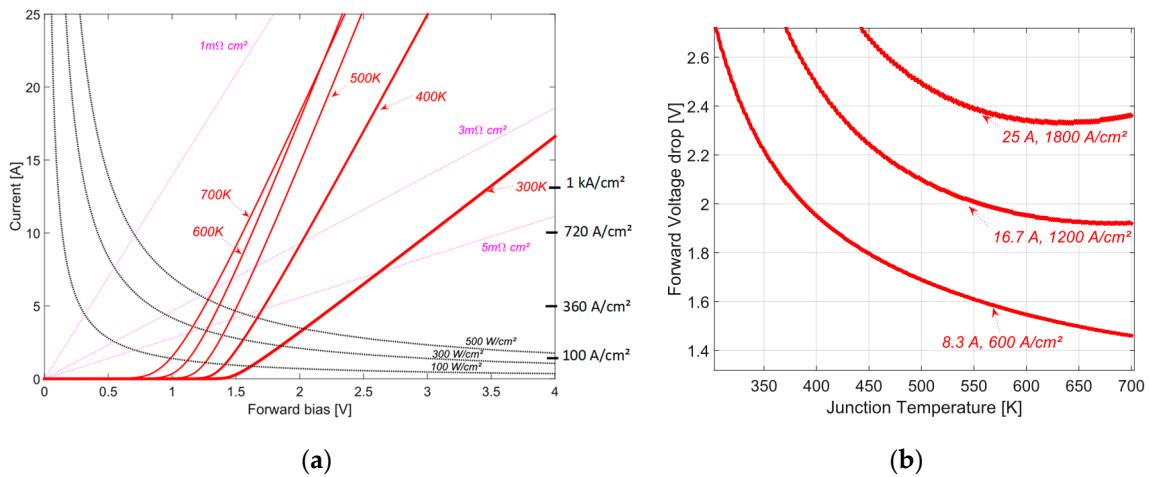


Figure 6. Forward characteristics for $[B] = 1.5 \times 10^{16} \text{ cm}^{-3}$ (Design Drift #c), $n = 1.2$ and $\Phi_b = 1.55 \text{ eV}$. (a) I-Vs for different temperatures. (b) Forward voltage drop as a function of temperature for three different constant current bias.

4. Design and Optimization of OFF-State

As previously discussed, the breakdown voltage of diamond diodes is limited by leakage currents due to thermionic emission and tunnelling mechanisms over and through the Schottky barrier rather than by avalanche effect. These leakage currents are enhanced by the presence of crystalline defects and by electric field crowding occurring at the edge of the main contact. Therefore, it is mandatory to use high crystalline quality diamond and efficient field relief structures to have a homogeneous distribution of the electrostatic potential on the surface, thus avoiding the premature breakdown of the device. In the absence of edge termination architectures, the maximum electric field is typically limited to values of the order of $3 \text{ MV}\cdot\text{cm}^{-1}$ as reported in [9,12,14,20,30,34], which suggests that improvements are still possible to reach the commonly cited value of $10 \text{ MV}\cdot\text{cm}^{-1}$ for the critical electric field of bulk diamond [35]. Consequently, it would be possible to extract physical parameters such as the avalanche impact ionization coefficients that remain experimentally unknown up to now.

Planar junction terminations formed by the ion implantation and diffusion of impurities cannot be applied to diamond due to irreversible structural defects generated during the ion implantation process [36]. Moreover, the lack of an efficient n-type doping (shallow donors) to form high quality pn

junctions in diamond prevents from developing efficient junction termination extension (JTE) unlike to other semiconductors (Si, SiC). Consequently, field plated SBDs using various oxides and geometries are reported in the literature [34,37–40]. However, they require oxide deposition, i.e., multiple lithography steps and a high oxide layer quality are needed. This has motivated the development of floating metal rings (FMRs) which efficiency on the reduction of the electric field is confirmed by electron beam induced current (EBIC) measurements such as reported in [32]. The efficiency of FMRs as field release structures was demonstrated on SiC and GaN devices for improving the BV [41–43]. Thus, it is natural to apply this technique to diamond due to the aforementioned reasons.

4.1. TCAD Simulations of OFF-State Diamond Diodes with FMR as Edge Termination

In order to design the OFF-state of diamond based unipolar devices and for considering the 3D effects (current distribution, electric field crowding), the material properties were implemented into the database of the TCAD Synopsys Sentaurus finite element based software [44]. The model parameters were adjusted to fit the diamond physical properties. Thus, the incomplete ionization was implemented by considering the temperature and doping dependence of the ionization energy of boron. The temperature and doping dependant mobility model was implemented through a C++ interpreter according to the semi-empirical model described in [24]. The reverse blocking characteristics were obtained by using the van Overstraeten-de Man avalanche generation model with the impact ionization coefficients taken from [23]. Finally, the Schottky barrier lowering effect was considered. All the models are described in more details in [25,45–47].

The oxygen terminated diamond surface is reproduced by setting the electron affinity to 1.7 eV [48]. The Schottky boundary conditions are defined thanks to the workfunction so that the Schottky barrier height is adjusted to the value of 1.7 eV (Mo interface [32]). The FMRs are of the same metal as the Schottky contact (cathode) and thus Schottky boundary conditions are applied to the FMRs. Imperfections such as charges or interface states at the Metal/Diamond interface, resulting in Fermi level pinning or Schottky barrier height inhomogeneities were not taken into account during the simulations. Their presence modifies the electrostatic potential distribution and consequently influences the breakdown voltage. Also, bulk defects having an influence on the reverse leakage currents were not considered. The latter were taken into account using non-local barrier tunnelling models with the tunnelling masses for electrons and holes $m_t = 0.5$ (default value) and the ratio between the semiconductor Richardson constant over the free electron Richardson constant $g = 0.75$. The barrier lowering effect which influences the magnitude of the reverse leakage currents was taken into account according to parameters reported in Ref. [47].

4.2. Design for 1kV Breakdown Voltage

Figure 7 shows the 2D axisymmetric device structure of the vertical diamond SBD without and with up to three FMRs. Two designs are considered which drift layer properties (1D BV and specific ON-state resistance) are summarized in Table 4. The following discussion considers only design #1. Drift layer design #2 will be used as a comparison in the next subsection when the number of rings will be considered as a parameter. The conductive substrate is represented by a 5 μm thick heavily boron-doped layer ($[B] = 2 \times 10^{20} \text{ cm}^{-3}$). The cathode with Schottky boundary conditions is defined on top of the drift layer and the anode with ohmic boundary conditions at the bottom of the structure. The expected BV of this 1D drift layer design is $BV_{1D} = 1070 \text{ V}$ as estimated by 1D analytical modelling [49].

Figure 8a represents the electric field distribution in the 2D structure at a reverse bias voltage of 200 V. The electric field maximum is located at the edge of the cathode. As soon as the FMR is added to the structure, this electric field peak at the cathode edge is decreased as highlighted in Figure 8b, which shows the electric field distribution in the structure for a single FMR located at $W_s = 0.15 \mu\text{m}$ from the cathode.

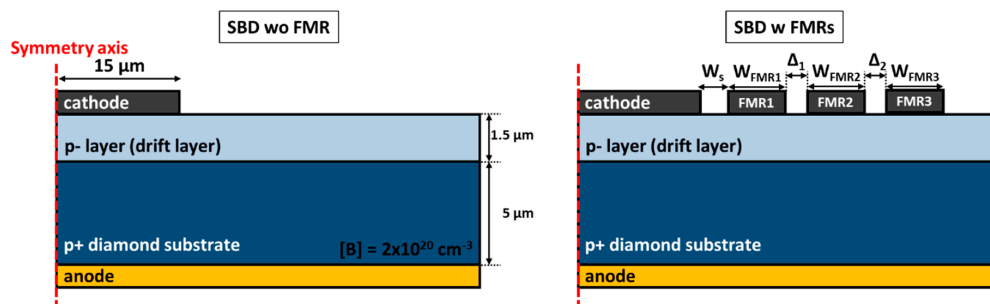


Figure 7. Cross-sectional view of the simulated diodes for a breakdown voltage design of 1.07 kV. W_s is the spacing between the cathode and FMR1, W_{FMRn} is the n^{th} ring width. Δ_1 is the gap between FMR1 and FMR2. Δ_2 is the gap between FMR2 and FMR3.

Table 4. Properties of the drift layer designs considered in this work.

1 kV Design	#1	#2
Drift layer thickness (μm)	1.5	1.5
Doping (cm^{-3})	1.5×10^{16}	2.1×10^{15}
1D BV (kV)	1.07	1.07
$R_{\text{on}S_{300\text{K}}} (\text{m}\Omega\cdot\text{cm}^2)$	2	6.3
$R_{\text{on}S_{500\text{K}}} (\text{m}\Omega\cdot\text{cm}^2)$	0.5	1.8

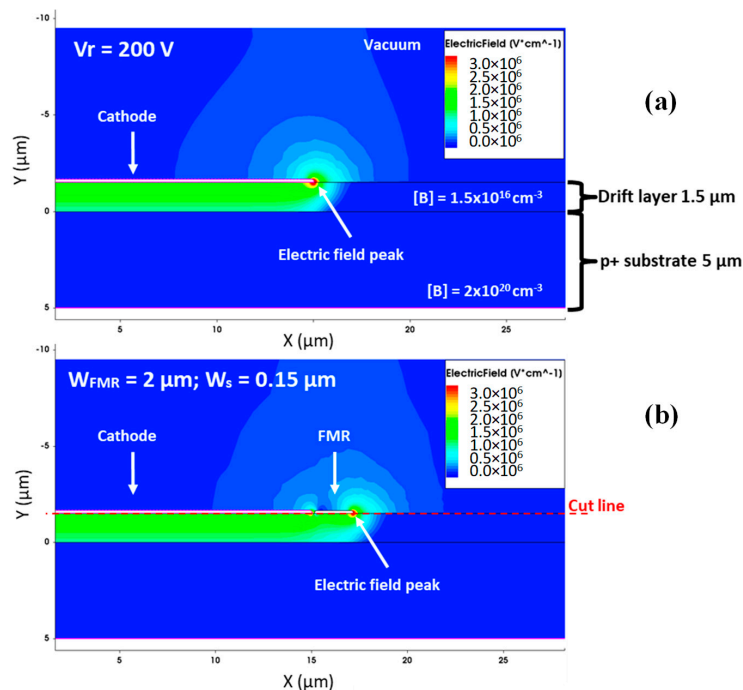


Figure 8. Electric field distribution in the 2D structure, at a reverse bias of 200 V (a) without FMR and (b) with a single FMR of width $W_{\text{FMR}} = 2 \mu\text{m}$. The spacing between the cathode and the ring is $W_s = 0.15 \mu\text{m}$.

Figure 9a represents the electric field profile along the cutline depicted in Figure 8b at a reverse bias voltage of 200 V. The distance between the cathode and the FMR influences the electric field peak at the edge of the cathode. In fact, its value reaches a minimum value for $W_s = 0.15 \mu\text{m}$. Figure 9b shows the simulated reverse leakage currents as a function of the reverse bias voltage at 300 K for the device structure without and with one FMR with several ring spacings. The BV of the device is defined when the current reaches a value of 10^{-6} A which corresponds to a current density of $0.14 \text{ A}\cdot\text{cm}^{-2}$ (in the order of tens of $\text{W}\cdot\text{cm}^{-2}$ power losses).

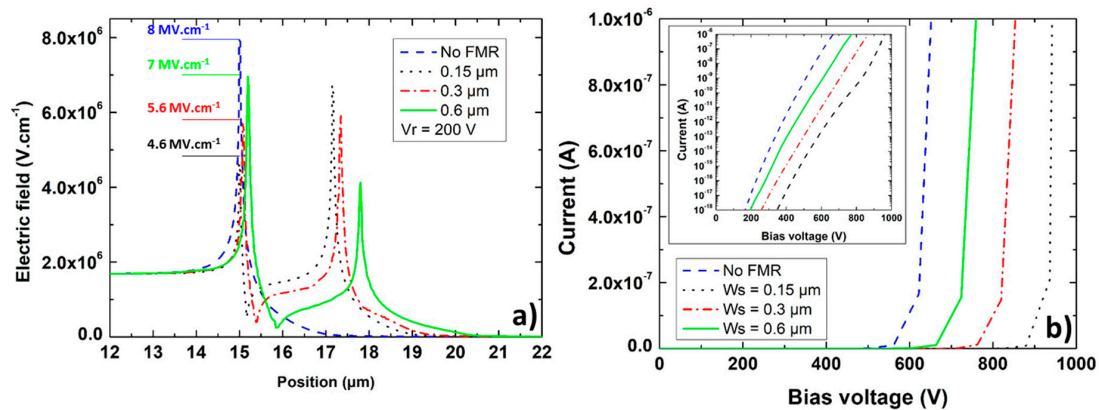


Figure 9. (a) Electric field profile as a function of the distance at a reverse bias voltage of 200 V performed along the cutline depicted in Figure 8b. The spacing between the FMR and the cathode influences the magnitude of the electric field peak at the edge of the cathode. (b) Simulated reverse leakage current as a function of the reverse bias voltage for the various configurations, without FMR and with one FMR. W_s is the spacing between the cathode and the FMR. The insert shows the reverse I-Vs in logarithmic scale. The simulated I-Vs are performed at 300 K. The BV is defined when the current in the structure reaches 10^{-6} A (0.14 A·cm $^{-2}$).

Thus, the termination efficiency depicted in Figure 10a reaches 93% of the 1D BV at 300 K when using a single FMR with parameters $W_s = 0.15$ μm and $W_{\text{FMR}} = 2$ μm . This termination efficiency drops to 79% at 500 K. However, this observation needs to be mitigated by the fact that the BV is normalized by the 1D analytical BV at 300 K. In fact, the analytical model does not take into account the temperature dependence of the impact ionization coefficients [49]. Figure 10b shows the BV improvement as a function of the ring spacing W_s normalized to the BV of the device without edge termination for 300 K and 500 K. One can notice that the optimum spacing between the first floating ring and the cathode, which is $W_s = 0.15$ μm , induces a high stress on the fabrication process and lithography. Therefore, it is necessary to consider the trade-off between either choosing a ring spacing of 0.3 μm and lower the BV of the device or adding FMRs. The latter is discussed in the next subsection.

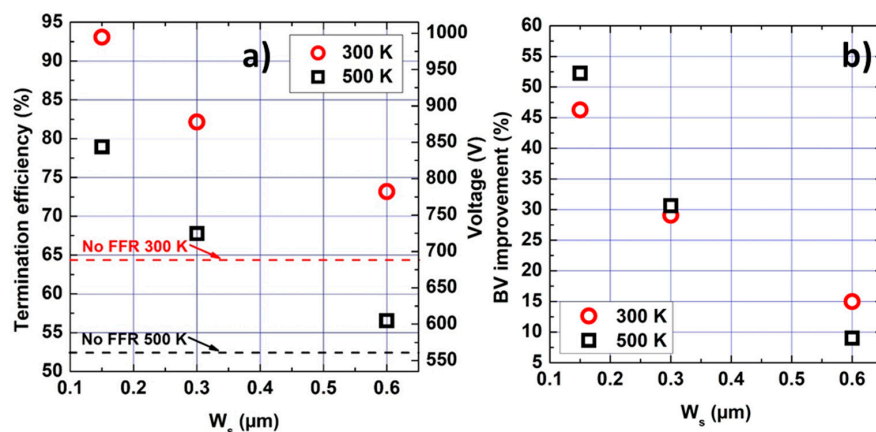


Figure 10. (a) Termination efficiency as a function of the ring spacing W_s . The termination efficiency is defined as the ratio between the 2D and the 1D BV at 300 K ($BV_{1D} = 1070$ V). The dotted lines represent the 2D BVs of the SBD without FMR which are 681 V and 555 V at 300 K and 500 K respectively. Here we defined the BV of the device when the total current in the structure reaches 10^{-6} A. (b) BV improvement obtained by comparing the BV of the device with and without FMR as a function of the ring spacing for 300 K and 500 K. The BV is improved by about 52% using $W_s = 0.15$ μm and $W_{\text{FMR}} = 2$ μm .

4.3. Influence of the Ring Number on the BV

Figure 11 shows the comparison between two devices with drift layer design #1: Figure 11a the structure with one FMR with $W_{\text{FMR}} = [2; 4] \mu\text{m}$ and Figure 11b with two FMRs with multiple combinations of ring widths. The two FMRs of various widths are separated by a distance of $\Delta_1 = 1 \mu\text{m}$, which is the optimized value leading to the best BV improvement. Using two FMRs improves the BV by approximately 57% (i.e., $BV_{1\text{FMR}} = 874 \text{ V}$, $BV_{2\text{FMRs}} = 869 \text{ V}$, $BV_{W_0\text{FMR}} = 555 \text{ V}$) as compared to the BV of the device without FMR. This is comparable to the improvement obtained with one FMR when using $W_s = 0.15 \mu\text{m}$ and $W_{\text{FMR}} = 4 \mu\text{m}$ as evidenced by Figure 11a. Thus, in this case increasing the number of FMRs in the design does not improve the BV of the device.

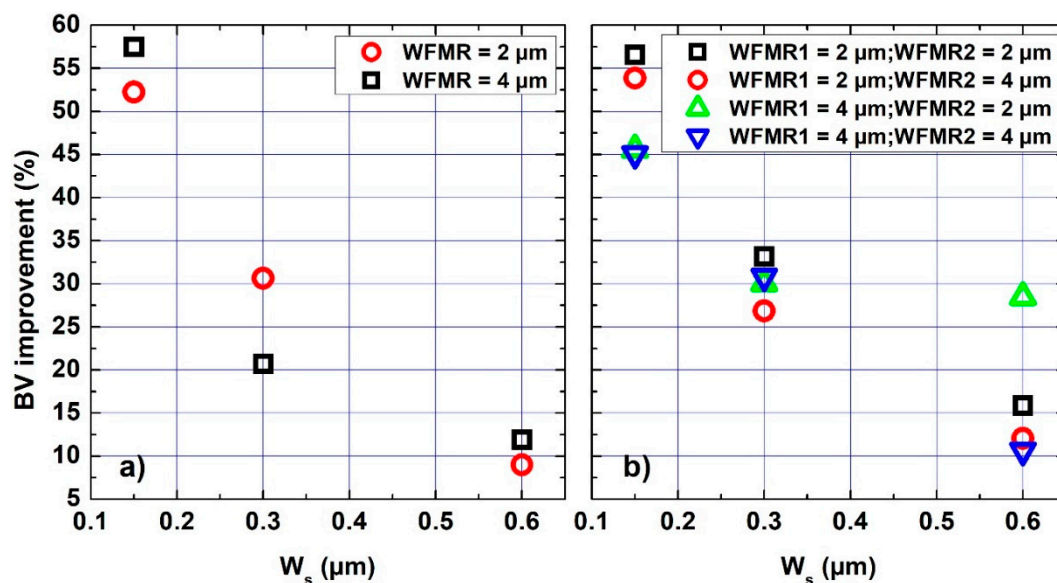


Figure 11. (a) BV improvements of design #1 for a single FMR at 500 K. (b) Using two FMRs, the improvement can reach up to 57% of the BV of the structure without FMR. The spacing between the two FMRs is $\Delta_1 = 1 \mu\text{m}$. The simulations were performed at 500 K.

The efficiency of the FMR in reducing the peak electric field strongly depends on the doping level of the drift region. In fact, the lateral extension of the depletion layer needs to punch through the FMR when a reverse bias is applied in order that it ends at the edge of the FMR instead of the cathode. Thus, Figure 12 compares the BV improvement using one and two FMRs for the drift layer design #2. The width of FMR1 and FMR2 is varied and the spacing between the two FMRs has a constant value of $\Delta_1 = 2 \mu\text{m}$, which is the optimized value. The drift layer design #2 has the same BV rating as design #1. However, the specific ON-state resistance is about three times larger than the one calculated for design #1, resulting from the lower doping level of $2.1 \times 10^{15} \text{ cm}^{-3}$ instead of $1.5 \times 10^{16} \text{ cm}^{-3}$, as shown in Table 4. From Figure 12b, it can be seen that in the optimum case, the BV can be improved by approximately 87% when using two FMRs, as compared to the device without field release structure (i.e., $BV_{1\text{FMR}} = 739 \text{ V}$, $BV_{2\text{FMRs}} = 911 \text{ V}$, $BV_{W_0\text{FMR}} = 487 \text{ V}$).

To complete the analysis, the ring number was increased up to three. In Figure 13, it can be seen that there is no need to increase the number of rings for drift layer design #1, since the BV improvement is almost constant for one and two rings and decreases when adding a third ring. On the other hand, the optimum number of rings for drift layer design #2 is two. In fact, the BV improvement reaches 87% when using two rings and drops to 69% when adding a third ring.

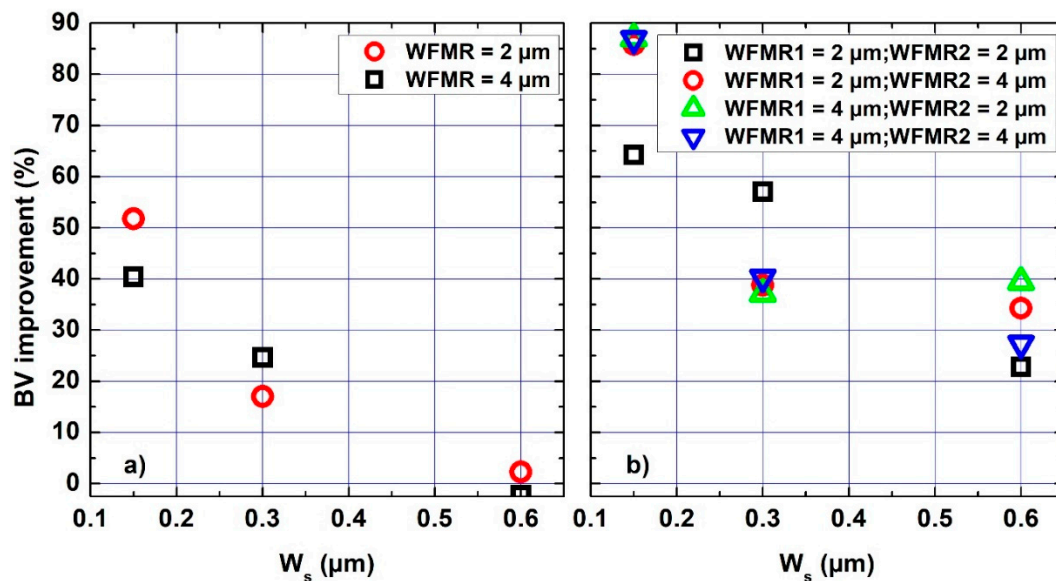


Figure 12. (a) BV improvements of design #2 for one FMR with two different widths. (b) Using two FMRs, the improvement can reach up to 87% of the BV of the structure without FMR. The spacing between the two FMRs is $\Delta_1 = 2 \mu\text{m}$. The simulations were performed at 500 K.

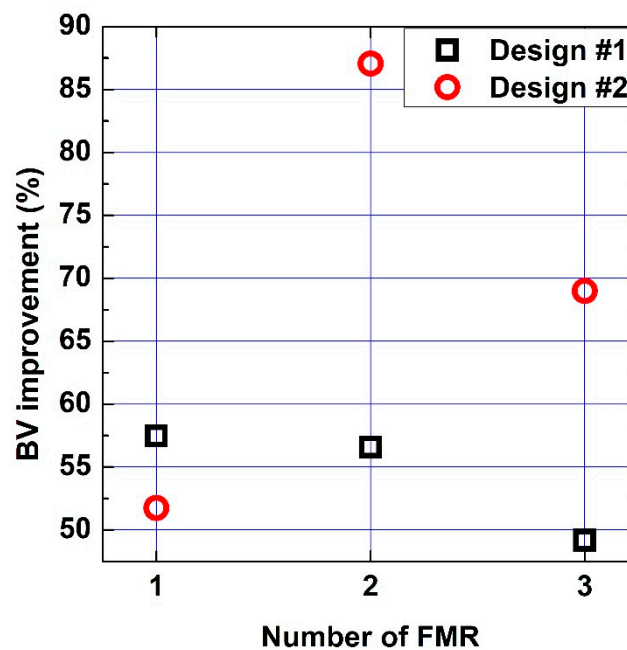


Figure 13. BV improvement as a function of the number of ring for drift layer design #1 and drift layer design #2.

The observation that increasing the number of ring for design #1 does not improve the breakdown seems to corroborate the EBIC measurements reported in Ref. [32], where the doping of the drift layer was in the range of 10^{16} cm^{-3} , comparable to design #1 ($1.5 \times 10^{16} \text{ cm}^{-3}$). It was observed that the EBIC signal was only significant over the first 4 rings on a SBD having 21 rings. Thus, it might not be relevant to develop diamond SBDs with a large number of FMRs. With design #2, two FMRs are required to obtain the largest BV, thanks an efficient reduction of the peak electric at the cathode edge and at the edges of both FMRs.

Finally, Table 5 summarizes the BV improvements and optimized BVs obtained for drift layer design #1 and drift layer design #2 in the case of a single FMR or multiple FMRs. Figure 14 shows the

consequent figure of merit for all considered designs: the design closest to the 1D theoretical limit at 500K is obtained with the higher drift region doping (design #2) and a single FMR, whereas the highest breakdown voltage is obtained with the lower drift region doping (design #1) and two FMRs.

Table 5. Optimized values for the two drift layer designs. BV improvement (%) and optimized BV (V) @ 500 K in the case of a single, two and three rings design respectively.

	Design #1			Design #2		
	Number of ring	1	2	3	1	2
BV improvement @ 500 K (%)	57.4	56.6	49.2	51.7	87	69
Optimized BV @ 500 K (V)	874	869	828	739	911	823

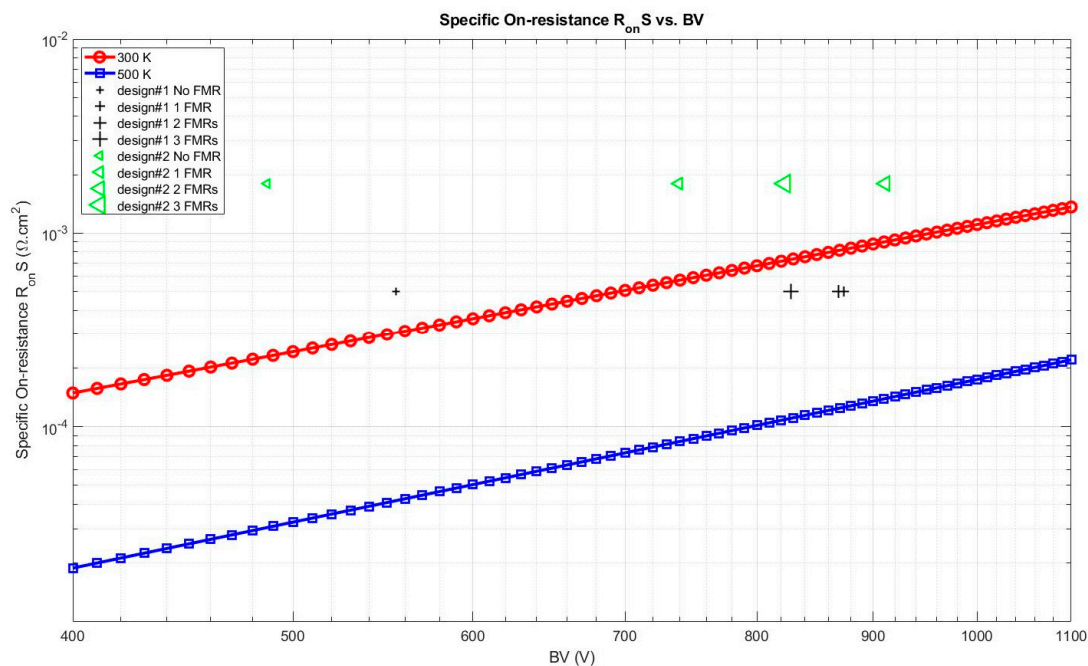


Figure 14. Figure of merit at 500 K for the two drift region designs and different edge terminations, also benchmarked with 1 D theoretical limit (300 K in red circles, 500 K in blue squares).

5. Conclusions

Thanks to the high critical electric field of diamond, the drift region doping level of diamond power devices can be largely increased. However, in the case of diamond Schottky diodes, this leads to possibly large leakage currents in the OFF state. The trade-off between the Schottky barrier height, drift region Boron doping level, ON-state current and power loss densities, OFF-state leakage current and power loss densities, and breakdown voltage has been presented and discussed. To further improve the figure of merits of diamond Schottky diodes, Floating Metal Rings (FMRs) have been designed, taking careful note of the fabrication challenges (e.g., rings widths and spacing). Thanks to the designed FMRs, the breakdown voltage at 500 K is improved from 487 V to 911 V, and a ON-state specific resistance of $0.5 \text{ m}\Omega\cdot\text{cm}^2$ is obtained at 500 K for a breakdown voltage of 869 V. Experimental investigations of optimized diamond Schottky diodes with FMRs are ongoing, while diamond models must also be continuously verified (e.g., impact ionization coefficients, leakage currents). With optimized designs and high-quality growth techniques, diamond devices will offer new opportunities for the power electronics community.

Author Contributions: Conceptualization, N.R.; methodology, N.R. and A.M.; writing—original draft preparation, A.M.; writing—review and editing, N.R. and A.M.; supervision, N.R.; project administration, N.R.; funding acquisition, N.R.

Funding: This research is partially funded by French ANR Research Agency under grant ANR-16-CE05-0023 #Diamond-HVDC. This work is supported by Laboratoire d'Excellence LANEF in Grenoble (ANR-10-LABX-51-01).

Acknowledgments: The authors thank D.E. from Institut Néel (Grenoble, France) for fruitful discussions on diamond Schottky diodes.

Conflicts of Interest: The authors declare no conflict of interest.

References

1. Geis, M.W.; Gregory, J.A.; Pate, B.B. Capacitance-voltage measurements on metal-SiO₂-diamond structures fabricated with (100)- and (111)-oriented substrates. *IEEE Trans. Electron Devices* **1991**, *38*, 619–626. [[CrossRef](#)]
2. Shiomi, H.; Nakahata, H.; Imai, T.; Nishibayashi, Y.; Fujimori, N. Electrical Characteristics of Metal Contacts to Boron-Doped Diamond Epitaxial Film. *Jpn. J. Appl. Phys.* **1989**, *28*, 758. [[CrossRef](#)]
3. Gildenblat, G.S.; Grot, S.A.; Wronski, C.R.; Badzian, A.R.; Badzian, T.; Messier, R. Electrical characteristics of Schottky diodes fabricated using plasma assisted chemical vapor deposited diamond films. *Appl. Phys. Lett.* **1988**, *53*, 586–588. [[CrossRef](#)]
4. Volpe, P.N.; Muret, P.; Pernot, J.; Omnès, F.; Teraji, T.; Koide, Y.; Jomard, F.; Planson, D.; Brosselard, P.; Dheilly, N.; et al. Extreme dielectric strength in boron doped homoepitaxial diamond. *Appl. Phys. Lett.* **2010**, *97*, 223501. [[CrossRef](#)]
5. Traoré, A.; Muret, P.; Fiori, A.; Eon, D.; Gheeraert, E.; Pernot, J. Zr/oxidized diamond interface for high power Schottky diodes. *Appl. Phys. Lett.* **2014**, *104*, 052105. [[CrossRef](#)]
6. Makino, T.; Tanimoto, S.; Hayashi, Y.; Kato, H.; Tokuda, N.; Ogura, M.; Takeuchi, D.; Oyama, K.; Ohashi, H.; Okushi, H.; et al. Diamond Schottky-pn diode with high forward current density and fast switching operation. *Appl. Phys. Lett.* **2009**, *94*, 262101. [[CrossRef](#)]
7. Traore, A.; Nakajima, A.; Makino, T.; Kuwabara, D.; Kato, H.; Ogura, M.; Takeuchi, D.; Yamazaki, S. Dynamic properties of diamond high voltage p-i-n diodes. *Jpn. J. Appl. Phys.* **2017**, *56*, 04CR14. [[CrossRef](#)]
8. Umezawa, H.; Shikata, S.; Funaki, T. Diamond Schottky barrier diode for high-temperature, high-power, and fast switching applications. *Jpn. J. Appl. Phys.* **2014**, *53*, 05FP06. [[CrossRef](#)]
9. Bormashov, V.S.; Terentiev, S.A.; Buga, S.G.; Tarelkin, S.A.; Volkov, A.P.; Teteruk, D.V.; Kornilov, N.V.; Kuznetsov, M.S.; Blank, V.D. Thin large area vertical Schottky barrier diamond diodes with low on-resistance made by ion-beam assisted lift-off technique. *Diam. Relat. Mater.* **2017**, *75*, 78–84. [[CrossRef](#)]
10. Umezawa, H.; Nagase, M.; Kato, Y.; Shikata, S. High temperature application of diamond power device. *Diam. Relat. Mater.* **2012**, *24*, 201–205. [[CrossRef](#)]
11. Makino, T.; Kato, H.; Tokuda, N.; Ogura, M.; Takeuchi, D.; Oyama, K.; Tanimoto, S.; Okushi, H.; Yamasaki, S. Diamond Schottky-pn diode without trade-off relationship between on-resistance and blocking voltage. *Phys. Status Solidi A* **2010**, *207*, 2105–2109. [[CrossRef](#)]
12. Suzuki, M.; Sakai, T.; Makino, T.; Kato, H.; Takeuchi, D.; Ogura, M.; Okushi, H.; Yamasaki, S. Electrical characterization of diamond PiN diodes for high voltage applications. *Phys. Status Solidi A* **2013**, *210*, 2035–2039. [[CrossRef](#)]
13. Blank, V.D.; Bormashov, V.S.; Tarelkin, S.A.; Buga, S.G.; Kuznetsov, M.S.; Teteruk, D.V.; Kornilov, N.V.; Terentiev, S.A.; Volkov, A.P. Power high-voltage and fast response Schottky barrier diamond diodes. *Diam. Relat. Mater.* **2015**, *57* (Suppl. C), 32–36. [[CrossRef](#)]
14. Kumaresan, R.; Umezawa, H.; Tatsumi, N.; Ikeda, K.; Shikata, S. Device processing, fabrication and analysis of diamond pseudo-vertical Schottky barrier diodes with low leak current and high blocking voltage. *Diam. Relat. Mater.* **2009**, *18*, 299–302. [[CrossRef](#)]
15. Oyama, K.; Ri, S.G.; Kato, H.; Ogura, M.; Makino, T.; Takeuchi, D.; Tokuda, N.; Okushi, H.; Yamasaki, S. High performance of diamond p+-i-n+ junction diode fabricated using heavily doped p+ and n+ layers. *Appl. Phys. Lett.* **2009**, *94*, 152109. [[CrossRef](#)]
16. Perez, G.; Lefranc, P.; Jeannin, P.; Eon, D.; Rouger, N. Parallel and interleaved structures for diamond Schottky diodes. In Proceedings of the 2017 19th European Conference on Power Electronics and Applications (EPE'17 ECCE Europe), Warsaw, Poland, 11–14 September 2017; pp. P.1–P.10.
17. Perez, G.; Chicot, G.; Avenas, Y.; Lefranc, P.; Jeannin, P.O.; Eon, D.; Rouger, N. Integrated temperature sensor with diamond Schottky diodes using a thermosensitive parameter. *Diam. Relat. Mater.* **2017**, *78*, 83–87. [[CrossRef](#)]

18. Matsumoto, T.; Mukose, T.; Makino, T.; Takeuchi, D.; Yamasaki, S.; Inokuma, T.; Tokuda, N. Diamond Schottky-pn diode using lightly nitrogen-doped layer. *Diam. Relat. Mater.* **2017**, *75*, 152–154. [[CrossRef](#)]
19. Makino, T.; Kato, H.; Takeuchi, D.; Ogura, M.; Okushi, H.; Yamasaki, S. Device Design of Diamond Schottky-pn Diode for Low-Loss Power Electronics. *Jpn. J. Appl. Phys.* **2012**, *51*, 090116. [[CrossRef](#)]
20. Dutta, M.; Koeck, F.A.M.; Li, W.; Nemanich, R.J.; Chowdhury, S. High Voltage Diodes in Diamond Using (100)- and (111)- Substrates. *IEEE Electron Device Lett.* **2017**, *38*, 600–603. [[CrossRef](#)]
21. Chicot, G.; Eon, D.; Rouger, N. Optimal drift region for diamond power devices. *Diam. Relat. Mater.* **2016**, *69*, 68–73. [[CrossRef](#)]
22. Baliga, B.J. *Fundamentals of Power Semiconductor Devices*; Springer: New York, NY, USA, 2008.
23. Hiraiwa, A.; Kawarada, H. Figure of merit of diamond power devices based on accurately estimated impact ionization processes. *J. Appl. Phys.* **2013**, *114*, 034506.
24. Volpe, P.-N.; Pernot, J.; Muret, P.; Omnès, F. High hole mobility in boron doped diamond for power device applications. *Appl. Phys. Lett.* **2009**, *94*, 092102. [[CrossRef](#)]
25. Maréchal, A.; Rouger, N.; Crebier, J.C.; Pernot, J.; Koizumi, S.; Teraji, T.; Gheeraert, E. Model implementation towards the prediction of J(V) characteristics in diamond bipolar device simulations. *Diam. Relat. Mater.* **2014**, *43* (Suppl. C), 34–42. [[CrossRef](#)]
26. Traoré, A.; Koizumi, S.; Pernot, J. Effect of n- and p-type doping concentrations and compensation on the electrical properties of semiconducting diamond. *Phys. Status Solidi A* **2016**, *213*, 2036–2043. [[CrossRef](#)]
27. Pernot, J.; Volpe, P.N.; Omnès, F.; Muret, P.; Mortet, V.; Haenen, K.; Teraji, T. Hall hole mobility in boron-doped homoepitaxial diamond. *Phys. Rev. B* **2010**, *81*, 205203. [[CrossRef](#)]
28. Koizumi, S.; Umezawa, H.; Pernot, J.; Suzuki, M. 3- Fundamental material's nature of diamond. In *Power Electronics Device Applications of Diamond Semiconductors*; Woodhead Publishing: Sawston, UK, 2018; pp. 191–217.
29. Koizumi, S.; Umezawa, H.; Pernot, J.; Suzuki, M. (Eds.) 5-Device formation and the characterizations. In *Power Electronics Device Applications of Diamond Semiconductors*; Woodhead Publishing: Sawston, UK, 2018; pp. 295–382.
30. Umezawa, H.; Saito, T.; Tokuda, N.; Ogura, M.; Ri, S.G.; Yoshikawa, H.; Shikata, S.I. Leakage current analysis of diamond Schottky barrier diode. *Appl. Phys. Lett.* **2007**, *90*, 073506. [[CrossRef](#)]
31. Traoré, A. High Power Diamond Schottky Diode. Ph.D. Thesis, Université de Grenoble, Grenoble, France, 2015.
32. Driche, K.; Rugen, S.; Kaminski, N.; Umezawa, H.; Okumura, H.; Gheeraert, E. Electric field distribution using floating metal guard rings edge-termination for Schottky diodes. *Diam. Relat. Mater.* **2018**, *82*, 160–164. [[CrossRef](#)]
33. CPW4-1200-S010B 1200V Z-Rec Schottky Diode|Wolfspeed [En ligne]. Available online: <https://www.wolfspeed.com/cpw4-1200-s010b> (accessed on 18 April 2019).
34. Umezawa, H.; Kato, Y.; Shikata, S. 1 Ω On-Resistance Diamond Vertical-Schottky Barrier Diode Operated at 250 °C. *Appl. Phys. Express* **2013**, *6*, 011302. [[CrossRef](#)]
35. Landstrass, M.I.; Plano, M.A.; Moreno, M.A.; McWilliams, S.; Pan, L.S.; Kania, D.R.; Han, S. Device properties of homoepitaxially grown diamond. *Diam. Relat. Mater.* **1993**, *2*, 1033–1037. [[CrossRef](#)]
36. Koizumi, S.; Umezawa, H.; Pernot, J.; Suzuki, M. (Eds.) 2-Doping and semiconductor characterizations. In *Power Electronics Device Applications of Diamond Semiconductors*; Woodhead Publishing: Sawston, UK, 2018; pp. 99–189.
37. Ikeda, K.; Umezawa, H.; Shikata, S. Edge termination techniques for p-type diamond Schottky barrier diodes. *Diam. Relat. Mater.* **2008**, *17*, 809–812. [[CrossRef](#)]
38. Nawawi, A.; Tseng, K.J.; Amaratunga, G.A.J.; Umezawa, H.; Shikata, S. Design and optimization of planar mesa termination for diamond Schottky barrier diodes. *Diam. Relat. Mater.* **2013**, *36*, 51–57.
39. Brezeanu, M.; Butler, T.; Rupesinghe, N.L.; Amaratunga GA, J.; Rashid, S.J.; Udrea, F.; Avram, M.; Brezeanu, G. Ramp oxide termination structure using high-k dielectrics for high voltage diamond Schottky diodes. *Diam. Relat. Mater.* **2007**, *16*, 1020–1024. [[CrossRef](#)]
40. Brezeanu, M.; Avram, M.; Rashid, S.J.; Amaratunga GA, J.; Butler, T.; Rupesinghe, N.L. Termination Structures for Diamond Schottky Barrier Diodes. In Proceedings of the 2006 IEEE International Symposium on Power Semiconductor Devices and IC's, Naples, Italy, 4–8 June 2006; pp. 1–4.

41. Gupta, S.K.; Pradhan, N.; Shekhar, C.; Akhtar, J. Design, Fabrication, and Characterization of Ni/4H-SiC (0001) Schottky Diodes Array Equipped with Field Plate and Floating Guard Ring Edge Termination Structures. *IEEE Trans. Semicond. Manuf.* **2012**, *25*, 664–672. [[CrossRef](#)]
42. Chang, S.-C.; Wang, S.-J.; Uang, K.-M.; Liou, B.-W. Design and fabrication of high breakdown voltage 4H-SiC Schottky barrier diodes with floating metal ring edge terminations. *Solid-State Electron.* **2005**, *49*, 437–444. [[CrossRef](#)]
43. Lee, S.C.; Ha, M.W.; Her, J.C.; Kim, S.S.; Lim, J.Y.; Seo, K.S.; Han, M.K. High breakdown voltage GaN Schottky barrier diode employing floating metal rings on AlGaN/GaN hetero-junction. In Proceedings of the ISPSD '05, 17th International Symposium on Power Semiconductor Devices and ICs, Santa Barbara, CA, USA, 23–26 May 2005; pp. 247–250.
44. Synopsys. *SentaurusTM Device User Guide*; Synopsys Inc.: Mountain View, CA, USA, 2015.
45. Donato, N.; Antoniou, M.; Napoli, E.; Amaratunga, G.; Udrea, F. On the models used for TCAD simulations of Diamond Schottky Barrier Diodes. In Proceedings of the 2015 International Semiconductor Conference (CAS), Sinaia, Romania, 12–14 October 2015; pp. 223–226.
46. Donato, N.; Pagnano, D.; Napoli, E.; Longobardi, G.; Udrea, F. Design of a normally-off diamond JFET for high power integrated applications. *Diam. Relat. Mater.* **2017**, *78*, 73–82. [[CrossRef](#)]
47. Nawawi, A. Study of Single Crystal Diamond Schottky Barrier Diodes for Power Electronics Applications. Ph.D. Thesis, Nanyang Technological University, Singapore, 2014.
48. Shirafuji, J.; Sugino, T. Electrical properties of diamond surfaces. *Diam. Relat. Mater.* **1996**, *5*, 706–713. [[CrossRef](#)]
49. Rouger, N. Electric field distribution and voltage breakdown modeling for any PN junction. *COMPEL* **2015**, *35*, 137–156. [[CrossRef](#)]



© 2019 by the authors. Licensee MDPI, Basel, Switzerland. This article is an open access article distributed under the terms and conditions of the Creative Commons Attribution (CC BY) license (<http://creativecommons.org/licenses/by/4.0/>).